Additive Decomposition of Shear Strength in Cohesive Granular Media from Grain-Scale Interactions

Alfredo Taboada, Nicolas Estrada, Farhang Radjai

Additive Decomposition of Shear Strength in Cohesive Granular Media from Grain-Scale Interactions

Alfredo Taboada,[1] Nicolas Estrada,[1] and Farhang Radjaı[2]

[1]*Laboratoire Dynamique de la Lithosphère, Université de Montpellier II, Batiment 22, cc060, Place Eugène Bataillon, 34095 Montpellier cédex 5, France*

[2]*LMGC, CNRS-Université de Montpellier II, Place Eugène Bataillon, 34095 Montpellier cédex 5, France*

We study cemented granular media by introducing cohesive bonding (sliding or rolling friction and tensile strength) between grains in the framework of the contact dynamics method. We find that, for a wide range of bond parameters, the macroscopic angle of friction at the peak state can be split into three distinct terms of collisional, frictional and dilational origins. Remarkably, the macroscopic tensile strength depends only on the bond tensile strength, and the friction angle at the peak state is proportional to the dilatancy angle which varies linearly with sliding friction.

Cohesive granular materials are of particular interest to various fields of science and engineering such as soil mechanics, geology, and processing of fine powders and grains. Although cohesive interactions can have very different physicochemical origins, their common denominator is to freeze, up to a threshold in force or torque, the relative degrees of freedom between grains. Besides the Coulomb friction, which is also present in cohesionless materials as the main source of shear strength, well-known examples of cohesive bonding are mineral cementation, capillarity, and van der Waals forces in dense or fine-grained materials [1,2].

From a grain-scale viewpoint, an interesting and largely open issue is how local force thresholds scale up to macroscopic strength properties (friction angle and cohesion). However, the influence of local thresholds can hardly be investigated by direct experiments. The thresholds are material dependent and therefore cannot be isolated and varied methodically. A unique opportunity is offered by capillary cohesion which can be controlled by liquid content [3–5]. For example, several studies have focused on the effect of the adhesion force on the maximum angle of stability [6].

On the other hand, discrete element simulations provide a suitable tool to investigate large scale properties from local parameters. Several numerical studies have been reported focusing mostly on the compaction and flow properties of cohesive granular materials [7–11]. We are aware of few numerical studies dealing in a systematic manner with the macroscopic strength properties [12,13].

In this Letter, we present a detailed analysis of the shear strength in cohesive packs simulated by the contact dynamics method. Parametric study leads to an appealing picture depicting the precise role of each bond parameter in the cohesive behavior. The model of cohesive bonding in the simulations was designed to mimic cohesion by cementation as observed in rocks and soils. It incorporates the following features : (1) cohesive interactions are governed by shear force and torque thresholds that are proportional to the normal force, as well as a tensile force threshold [Fig. 1(a)]; (2) cohesive bonding occurs inside a small zone between grains, representing in a way the cementing material [Fig. 1(b)]; (3) contact rupture leads to an irreversible loss of tensile strength (debonding) and the contact turns to purely frictional behavior.

In the following, we attribute positive values to compressive forces. By definition, the tensile force threshold $-F_a$ is the largest tensile force that can be supported by a pair of grains along the contact normal. It is also useful to introduce a tensile stress $\sigma_a \equiv F_a/\ell$ where ℓ is the mean diameter of the grains in contact. For sliding friction, we use Coulomb's law in which the shear force threshold $T_{\max}$ is given by

$$T_{\max} = \mu_s(N + F_a), \tag{1}$$

where μ_s is the coefficient of sliding friction and N is the normal force. The offset $\mu_s F_a$ can be interpreted as the effect of adhesion forces increasing the contact area and thus the resistance to sliding.

Full cementation requires also torque transmission at the contact points. This is equivalent to a rolling resistance with possibly a torque threshold $\Gamma_{\max}$. We assume that $\Gamma_{\max}$ obeys a Coulomb-like law [14]

$$\Gamma_{\max} = \mu_r \ell(N + F_a), \tag{2}$$

where μ_r is the coefficient of rolling friction. Obviously, the length scales involved in the description of rolling resistance are those of the cohesive bond. In grain-scale numerical simulations, however, it is not desirable to in-

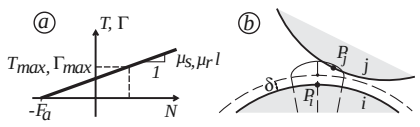

FIG. 1. (a) Shear and torque failure envelopes and (b) cohesive bond.

troduce small length scales compared to grain size. In Eq. (2), the presence of ℓ is simply meant to make μ_r dimensionless. At the particle scale, μ_s, μ_r, and σ_a represent the microscopic parameters of the model that express at this scale the underlying physicochemical properties of the contact interactions.

The kinetics of contact loss and gain is governed by a creation length δ and an elliptic zone of weak extension located between the grains; see Fig. 1(b). The cohesive bonds are created initially between all grains such that the gap, i.e., the distance between their two closest material points P_i and P_j, is below δ. A cohesive bond persists as long as the point P_j is located inside a small elliptical zone fixed to disk i. The parameter δ and the size of the elliptic zone simply control the scale of strain softening and they do not influence the results presented below as far as they remain small compared to the average particle size.

The simulations are based on the contact dynamics method [15,16]. Specific implementation for cohesionless materials can be found elsewhere [17]. Numerical samples are composed of 5000 disks with diameters uniformly distributed by volume fraction between 1 m and 4 m. The gravity is zero and, as for most geomaterials, the restitution coefficients are set to zero. The packing is built according to simple geometrical rules inside a rectangular cell and then uniaxially compacted with zero friction in order to produce a dense disordered configuration [17]. We get a volume fraction $\nu = 0.84$ and a coordination number $Z = 3.9$.

Before shearing, the two vertical walls are removed and the confining pressure is applied directly on the disks located at the boundaries of the sample [17]. The packing is sheared as in a biaxial test by downward displacement of the top wall for different values of the confining pressure σ_3. Simulations were performed for the following set of contact parameters: $\mu_s \in [0.01, 0.1, \ldots, 0.6]$, $\mu_r \in [0, 0.1, 0.25]$, $\sigma_a \in [0, 1, 2, 4, 10, 20]$ MPa.

Figure 2 displays typical stress-strain and volumetric strain plots at different levels of confinement. The stress ratio σ_1/σ_3, where σ_1 is the stress along the compression axis, first rises to a peak in a rigid fashion and then gradually declines with the shear strain $\epsilon_q \equiv \epsilon_1 - \epsilon_3$, where ϵ_1, ϵ_3 are major and minor cumulative strains. The peak stress ratio is a decreasing function of the confining pressure, as also observed in soil mechanics [18]. This behavior reflects a decrease of the effective level of cohesion σ_a/σ_3. In all tests, the stress ratio declines to the same constant residual strength for $\epsilon_q > 0.1$, corresponding to a permanent loss of cohesion along the shear bands in this state. The plots of the volumetric strain $\epsilon_p \equiv \epsilon_1 + \epsilon_3$ show dilatant behavior due to the initially high solid fraction.

Our simulation data are fit well to the Mohr-Coulomb model. In other words, the failure envelope of Mohr circles constructed in the stress space (σ, τ), where σ and τ are, respectively, the normal and shear stresses, is a straight line (see inset to Fig. 5). For each combination of bond pa-

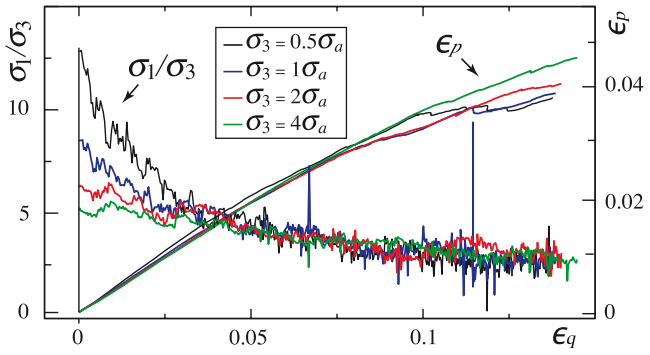

FIG. 2 (color online). Shear stress (a) and volumetric strain (b) as a function of shear strain at various confinement levels.

rameters, we determined the angle of friction ϕ_P (the slope of the failure line) and the cohesion C_P (intersection with the τ axis) at the peak state. We also determined the angle of friction ϕ_R for the residual state (the cohesion C_R being zero in this state), as well as the dilatancy angle $\psi \equiv \sin^{-1}(\delta\epsilon_p/\delta\epsilon_q)$ at the peak state.

Figure 3 shows ϕ_P and ϕ_R as a function of the sliding friction angle $\phi_s \equiv \tan^{-1}(\mu_s)$ for three values of the coefficient of rolling friction μ_r. Each symbol and the corresponding error bar represent the mean and extreme values of ϕ_P and ϕ_R for six different values of the tensile strength σ_a. A remarkable feature of these plots is that the macroscopic friction angles ϕ_P and ϕ_R are independent of the tensile strength as the variability is small around the mean values. Both ϕ_P and ϕ_R increase with μ_r.

As ϕ_s tends to zero, both angles of friction tend to a finite value ϕ_0 lying between 4° and 7°. This shows that contact friction is not the only source of frictional behavior at the macroscopic scale. Energy dissipation in this "frictionless" limit can take place only as a result of inelastic collisions through unstable particle rearrangements. Dissipation by inelastic collisions being proportional to

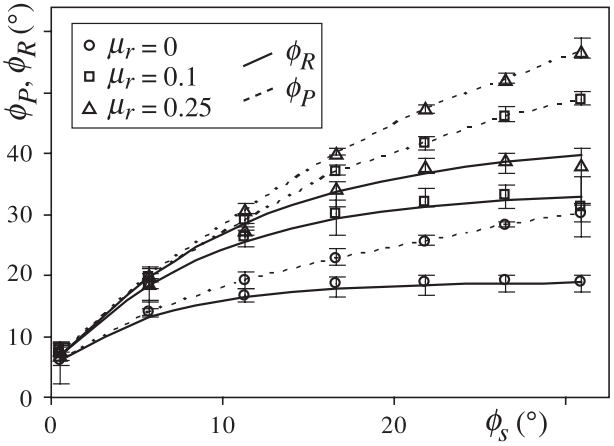

FIG. 3. Peak and residual friction angles ϕ_P and ϕ_R as a function of sliding friction angle ϕ_s. Full lines (ϕ_R) represent exponential fits whereas dashed lines (ϕ_P) join data points.

the mean stress, its effect appears as a Coulomb-like friction law with an apparent angle of friction ϕ_0.

The residual angle of friction ϕ_R increases with ϕ_s from ϕ_0 and saturates to a value ϕ_∞ that depends only on the rolling friction μ_r. The data are well fit to an exponential function:

$$\phi_R = \phi_0 + (\phi_\infty - \phi_0)(1 - e^{-\alpha\phi_s}), \tag{3}$$

with $\alpha \simeq 0.1$. Remark that, within statistical precision, α is independent of μ_r. The nonlinear dependence of ϕ_R on ϕ_s is consistent with other simulations reported in the past for $\mu_r = 0$ [19,20]. The saturation of ϕ_R suggests that, as ϕ_s increases, a transition occurs in the grain-scale phenomena underlying macroscopic friction. In particular, sliding and rolling appear to be the dominant deformation modes at low and high sliding frictions, respectively. It is a basic observation that the stress-strain behavior is strongly dependent on the initial value of the solid fraction. Only the so-called ''critical state,'' reached at large shear strains, is independent of the initial state [18]. This ''critical state'' is such that the stress ratio σ_1/σ_3 is constant and the dilatancy angle is zero on average. Thus, the strength parameter ϕ_R in the critical state should be considered as a material property.

On the other hand, the peak strength ϕ_P reflects the initial compactness of the material: higher dilatancy and peak friction angles are expected for higher initial compactness of the material. To check this correlation directly from numerical data, we plot in Fig. 4(a) the dilatancy angle ψ at the peak state as a function of the difference between peak and residual friction angles $\Delta\phi = \phi_P - \phi_R$. We observe a nice linear dependence with a slope close to 1. This indicates that the difference between peak and residual friction angles is fully explained by dilatancy. The dilatancy angle ψ for $\Delta\phi = 0$ corresponds to the macroscopic friction angle ϕ_0 for frictionless particles (see Fig. 3). Both, ψ and $\Delta\phi$, are nearly linear functions of ϕ_s and are barely influenced by μ_r [Fig. 4(b)]. Hence, with a good approximation, the dilatancy angle can be split into two parts:

$$\cong \phi_0 + \Delta\phi \cong \phi_0 + k\phi_s, \tag{4}$$

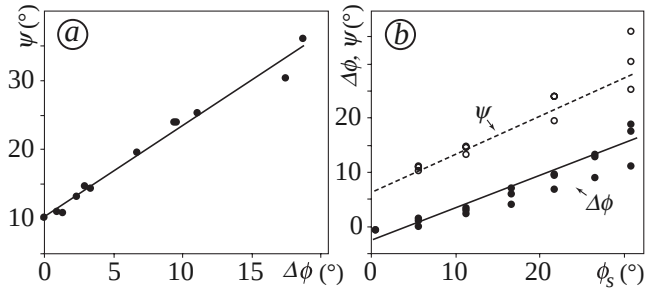

FIG. 4. (a) Dilatancy angle ψ as a function of $\Delta\phi$; (b) ψ and $\Delta\phi$ as a function of the angle of sliding friction ϕ_s; see the text for definitions.

with $k \simeq 0.5$. This remarkable correlation between friction and dilatancy angles, here verified for a cohesive granular material, is in agreement with Taylor's model proposed for cohesionless sand and known as stress-dilatancy relation [18].

We now consider the Coulomb cohesion C_P with respect to the influence of bond parameters. For reasons that will become clear below, we focus on the ''theoretical'' tensile stress $A^* \equiv C_P/\mu_P$ obtained by extrapolating the Mohr-Coulomb envelope from the compressional regime to the tensile regime (see inset in Fig. 5) [21].

Figure 5 shows A^* as a function of the local tensile strength σ_a. Each symbol and the corresponding error bar represent the mean and extreme values of A^* for the whole set of sliding and rolling frictions. We observe a linear dependence of the macroscopic tensile strength A^* on σ_a:

$$A^* \simeq \beta\sigma_a, \tag{5}$$

with $\beta \simeq 1.4$. Interestingly, A^* is independent of both sliding and rolling frictions. This feature may be explained by considering the stress on a plane perpendicular to the direction of extension and remarking that the friction forces and torques from contacts oriented along different directions cancel out along this direction [5,21]. This shows that the macroscopic strength parameters have different local origins. Local friction coefficients and inelastic collisions are responsible for the macroscopic friction, whereas the tensile strength at the contact scale seems to be the unique origin of macroscopic tensile strength.

The picture arising from this parametric study is both simple and rich. Equations (3) and (4) suggest an *additive partition* of the friction angles as illustrated in Fig. 6. In particular, the peak friction angle ϕ_P is expressed as a sum of three terms of different origins:

$$\phi_P = \phi_0 + \phi_\mu + \Delta\phi \cong \phi_\mu + \psi. \tag{6}$$

The offset ϕ_0 is a purely *collisional* contribution independent of rolling friction and tensile strength. The term $\phi_\mu \equiv \phi_R - \phi_0$ represents a purely *frictional* contribution. It is an exponential function of ϕ_s and saturates to $\phi_\infty - \phi_0$

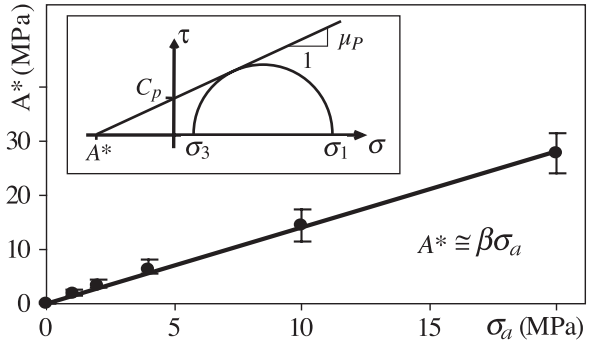

FIG. 5. Macroscopic theoretical tensile strength A^* (see inset) as a function of bond tensile strength σ_a.

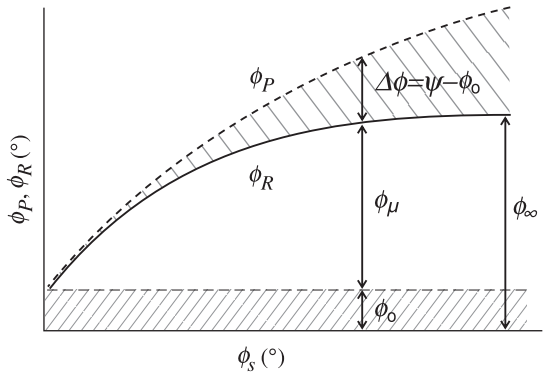

FIG. 6. Schematic representation of the partition of the peak angle of friction.

which increases with rolling friction μ_r. The term $\Delta\phi \equiv -\phi_0$ represents the contribution of *dilatancy* to the shear strength and, according to Eq. (4), it is an approximately linear function of ϕ_s.

In the same way, from Eqs. (5) and (6), the Coulomb cohesion can be expressed by a simple form:

$$C_P \cong \beta\sigma_a\mu_P \cong \beta\sigma_a \tan(\phi_0 + \phi_\mu + k\phi_s). \qquad (7)$$

This writing shows that the Coulomb cohesion is an increasing function of all bond parameters, the basic contribution coming from the tensile strength as a multiplicative factor. It is noteworthy that the cohesion in the limit $\phi_s = \phi_r = 0$ appears here to be a consequence of the collisional friction angle ϕ_0, i.e., $C_P = \beta\sigma_a \tan\phi_0$. In the absence of this term, the packing would behave as a cohesionless material independently of the local tensile strength σ_a. The constant β is likely to depend strongly on the distribution of cohesive bonds in the initial state. In particular, the fraction of cohesive bonds decays in inverse proportion to the solid fraction, suggesting that β will decrease dramatically in loose packings. The same is true for the parameter k relating ψ to ϕ_s. The dilatancy varies with the initial value of the solid fraction so that we expect lower values of k down to zero when the solid fraction is decreased to the critical state solid fraction.

The well-defined partition of the macroscopic angles of friction for a wide range of sliding and rolling friction coefficients at the contact scale in cohesive granular media is a key finding of the present investigation. In view of the large number of independent numerical tests performed, this result provides a solid basis for further insight into the behavior of cohesive granular media. Along these lines, a more detailed analysis of the respective roles of the sliding and rolling friction with respect to the frictional term ϕ_μ merits further investigation. It is also important to consider less compact configurations than those studied in this work. Finally, the evolution of granular microstructure up to and beyond the peak state is a crucial issue for understanding the scale up of bond interactions. On more general grounds, some quantitative correlations discussed in this Letter might turn out to be closely related to the underlying model of cohesive bonding. But, we believe that the partition of the Mohr-Coulomb strength parameters ϕ_P, ϕ_R, and C_P into collisional, frictional, and dilational parts, and the role of the local tensile strength as the unique source of the macroscopic tensile strength, are robust features of cohesive granular materials with respect to the model of cohesive bonding.

We thank K.-J. Chang for contribution to numerical simulations and A. Delplanque for technical help.

[1] J. C. Santamarina, in *Soil Behavior and Soil Ground Construction, A Symposium in Honor of Charles C. Ladd* (MIT, Cambridge, MA, 2001).
[2] M. M. Kohonen, D. Geromichalos, M. Scheel, C. Schier, and S. Herminghaus, Physica (Amsterdam) **A339**, 7 (2004).
[3] P. Pierrat and H. S. Caram, Powder Technol. **91**, 83 (1997).
[4] T. Kim and C. Hwang, Engineering Geology **69**, 233 (2003).
[5] V. Richefeu, M. S. E. Youssouffi, and F. Radjaï, Phys. Rev. E **73**, 051304 (2006).
[6] T. C. Halsey and A. J. Levine, Phys. Rev. Lett. **80**, 3141 (1998).
[7] C. Thornton, M. T. Ciomocos, and M. J. Adams, Powder Technol. **140**, 258 (2004).
[8] M. J. Rhodes, X. S. Wang, M. Nguyen, P. Stewart, and K. Liffman, Chem. Eng. Sci. **56**, 4433 (2001).
[9] T. Mikami, H. Kamiya, and M. Horio, Chem. Eng. Sci. **53**, 1927 (1998).
[10] M. J. Jiang, S. Leroueil, and J. M. Konrad, Computers and Geotechnics **31**, 473 (2004).
[11] T. Gröger, U. Tüzün, and D. M. Heyes, Powder Technol. **133**, 203 (2003).
[12] J.-Y. Delenne, M. S. E. Youssoufi, F. Cherblanc, and J.-C. Bénet, International Journal for Numerical and Analytical Methods in Geomechanics **28**, 1577 (2004).
[13] P. G. Rognon, J. N. Roux, D. Wolf, M. Naaim, and F. Chevoir, Europhys. Lett. **74**, 644 (2006).
[14] F. Radjaï, I. Preechawuttipong, and R. Peyroux, in *Continuous and Discontinuous Modelling of Cohesive Frictional Materials*, edited by P. A. Vermeer, S. Diebels, W. Ehlers, H. J. Herrmann, S. Luding, and E. Ramm (Springer, New York, 2001).
[15] J. J. Moreau, European Journal of Mechanics, A/Solids (Suppl.) **13**, 93 (1994).
[16] M. Jean, *Mechanics of Geometrical Interfaces* (Elsevier, New York, 1995), pp. 463–486.
[17] A. Taboada, K.-J. Chang, F. Radjai, and F. Bouchette, J. Geophys. Res. **110**, B09202 (2005).
[18] D. M. Wood, *Soil Behaviour and Critical State Soil Mechanics* (Cambridge University Press, Cambridge, England, 1990).
[19] L. Oger, S. B. Savage, D. Corriveau, and M. Sayed, Mech. Mater. **27**, 189 (1998).
[20] J. Lee and H. J. Herrmann, J. Phys. A **26**, 373 (1993).
[21] M. S. El Youssoufi, J.-Y. Delenne, and F. Radjaï, Phys. Rev. E **71**, 051307 (2005).